ROYAL SOCIETY
OF CHEMISTRY

PAPER

Check for updates

Comprehensive study of ultrathin TiN films by ALD: influence of film thickness and substrate on composition, structure, sheet resistance and durability

Kaushik Baishya, [ab] Luděk Hromádko,[a] Jan Brodský,[cd] Raul Zazpe, [*ab] Jhonatan Rodriguez-Pereira [ab] and Jan M. Macak [*ab]

This study investigates ultrathin titanium nitride (TiN) films in terms of their crystallographic structure, surface chemistry, sheet resistance and mechanical durability. These TiN ultrathin films were created by Atomic Layer Deposition (ALD) using $TiCl_4$ and NH_3 as precursors. The process consisted of 100, 200, 300 and 400 deposition cycles yielding ultrathin films 4.7, 9.4, 14.1 and 18.8 nm in thickness, respectively. Different planar substrates were employed, namely Si wafers, soda lime glasses and Ti foil. Based on image analyses, the deposition rate of 0.047 nm per cycle for ALD TiN (at 400 °C) was determined. A sheet resistance of 287 $\Omega/\square$ was achieved for the 18.8 nm film. X-ray diffraction (XRD) analysis confirmed the formation of cubic TiN with increasing crystallinity and texture with increased thickness. Sputter depth profiling in tandem with X-ray photoelectron spectroscopy (XPS) distinguished the uppermost oxidized surface from the stoichiometric TiN core in the films. Scratch tests demonstrated an enhanced adhesion and scratch resistance with ALD TiN films, aligned with the observed microstructural improvements. The comprehensive correlation between the film thickness, and their chemical composition, crystalline structure and mechanical performance highlights the vital role of ALD parameters in preparing TiN thin films for advanced technological applications.

1. Introduction

Titanium nitride (TiN) exhibits many favorable properties, in particular excellent mechanical hardness, and good thermal and electrical conductivities.[1] Thus, TiN has been employed in numerous applications, such as hard wear-resistant coatings,[2] as an excellent diffusion barrier in Ultra-Large Scale Integration (ULSI) technologies, and as a material for capacitor electrodes in Dynamic Random Access Memory (DRAM).[3,4] Also, the catalytic properties of TiN have gained significant interest due to its unique surface chemistry and electronic structure. These properties can be suitable for applications, such as ammonia synthesis, nitrogen fixation, and the oxygen reduction reaction. Due to their potential to serve as a cost-effective alternative to precious metal catalysts, TiN-based catalysts have been recently explored for sustainable industrial applications.[5–8]

Thin films of TiN can be prepared using a wide range of vacuum deposition processes, such as reactive magneton sputtering,[9–13] molecular-beam epitaxy,[14,15] chemical vapor deposition (CVD),[3,16–18] physical vapor deposition (PVD) including pulsed laser deposition (PLD)[19,20] and also the sol–gel process[21] under a nitrogen or ammonia atmosphere. Due to its excellent hardness and chemical resistance, etching TiN is challenging for micro or nanostructuring using conventional techniques, such as dry etching.[22] TiN films grown by CVD suffer from severe Cl contamination due to the use of $TiCl_4$ as a Ti precursor, which brings down the lifetime of the integrated circuit due to the corrosive nature of Cl.[23,24] Also, CVD often requires elevated temperatures (600–1000 °C) and there are challenges in regulating the thickness and morphology of the developing films.[25] Similarly, TiN films produced by PVD lack step coverage and homogeneity,[19,20] and often suffer from variations in the crystalline structure and texture, which can impact their performance.[26] In addition, Plasma-Enhanced CVD (PE-CVD) operates at lower temperatures, compared to thermal CVD, and there is still a need for substrate heating to ensure good quality films, which may limit the use of temperature-sensitive substrates.[19]

[a]*Center of Materials and Nanotechnologies, Faculty of Chemical Technology, University of Pardubice, Nam. Cs. Legii 565, 530 02 Pardubice, Czech Republic. E-mail: raul.zazpe@upce.cz; jan.macak@upce.cz*

[b]*Central European Institute of Technology, Brno University of Technology, Purkynova 123, 612 00 Brno, Czech Republic*

[c]*Department of Microelectronics, Faculty of Electrical Engineering and Communication, Brno University of Technology, Technická 3058/10, Brno, 61600, Czech Republic*

[d]*Department of Chemistry and Biochemistry, Mendel University in Brno, Zemědělská 1, 61300, Brno, Czech Republic*

In contrast, Atomic Layer Deposition (ALD) overcomes the limitations of the above-mentioned deposition techniques and enables precise control of film thickness, based on self-limiting film growth, conformal and uniform coating, and reduction of particle formation.[27–36] Studies have reported variation of electrical and physical properties of ALD TiN, prepared from different precursors, using different numbers of ALD cycles and deposition temperatures. For instance, the ALD TiN film at 425 °C using $TiCl_4$ showed a resistivity of ~200 μΩ cm.[37] Another study reported the use of an optimized thermal NH_3-based process with a growth rate of 0.06 nm per cycle and a resistivity value of 53.10^3 μΩ cm.[29] TiN films prepared by ALD using $TiCl_4$ and highly pure NH_3 (99.999%) show appreciably low film resistivity (~200 μΩ cm) under optimum deposition conditions.[30] In another study, ALD TiN films prepared using TEMATi at 425 °C showed the lowest carbon content and lowest resistivity (~220 μΩ cm) compared to other metal−organic Ti precursors.[31] Use of hydrazine (N_2H_4) as a promising N source to replace traditional NH_3 for ALD of TiN films to achieve low-resistivity has been studied.[38,39] Another study reported that an increase in the NH_3 flow from 500 to 4000 sccm led to a drop in the resistivity values of approximately 20%, while the TiN hardness and modulus increased by 75% and 40%, respectively.[32] Also, the ~40 nm thick TiN layer deposited by Plasma-Enhanced ALD (PE-ALD) can achieve consistent uniformity, maintaining sheet resistance ($R\square$) > 95% across a 6-inch wafer.[40] On the other hand, avoiding plasma can help to protect temperature-sensitive substrates from damage.

However, all the mentioned studies discussed ALD of TiN mostly on Si wafers. Actually, a comparison of the structure, oxidation, sheet resistance and mechanical stability among ALD TiN ultrathin films (below 20 nm) has not been explored yet. Such studies can provide a thickness-dependent evolution of the ALD TiN films' properties. In this work, we deposited ultrathin TiN films by ALD using 100, 200, 300, and 400 cycles on different substrates, including Si wafers, soda lime glasses and Ti foil. We performed a detailed analysis of the physical, electrical, and mechanical properties of these ultrathin TiN films and the impact of surface oxidation on these properties. Differences in crystallinity and texture as a function of the type of substrate are discussed. Moreover, scratch tests on ALD TiN films are reported for the first time in this study, to the best of the authors' knowledge. Overall, these results will provide insights for better understanding of ALD ultrathin TiN film behavior and the potential application limits.

2. Experimental section

2.1. Preparation of Si wafers, Ti foil and soda lime glasses

The Si wafer, soda lime glass and Ti foil substrates were cleaned using the following cleaning protocol before ALD processes. The substrates were dipped in acetone, isopropanol and distilled water under sonication for 5 min for each solvent and finally dried by blowing N_2.

2.2. Atomic layer deposition of TiN

ALD of TiN thin films (Beneq-TFS 200) was carried out at a deposition temperature of 400 °C with a base pressure of approximately 2 mbar using $TiCl_4$ (99.99+%, STREM) as a Ti precursor and NH_3 as the N precursor. N_2 (99.9999%) was used as a carrier gas applying a flow rate of 500 standard cubic centimeters per minute (sccm) in a continuous flow process. One ALD cycle was composed of the following sequence: $TiCl_4$ pulse (500 ms)- purge (4 s)-NH_3 pulse (2.5 s)- purge (5 s)-NH_3 pulse (2.5 s)- purge (5 s). Accordingly, cleaned Si wafers with native SiO_2, soda lime glasses, and Ti foil were coated with 100, 200, 300, and 400 ALD cycles of TiN, and are denoted as 100c, 200c, 300c, and 400c in the study. A thicker film with 600c ALD TiN was produced on a Si wafer as shown in the cross-sectional SEM image in Fig. S1. The thickness of this ALD TiN layer was statistically evaluated to be ~28 nm and the growth rate of ALD TiN at 400 °C was therefore calculated to be ≈0.047 nm per cycle. Hence, the calculated thickness values of 100c, 200c, 300c and 400c ALD TiN are 4.7, 9.4, 14.1 and 18.8 nm, respectively.

The evaluation of the morphology and the thickness of the 100c, 200c, 300c and 400c ALD TiN thin films on the different substrates was conducted using a field-emission scanning electron microscope (SEM, JEOL JSM 7500F). SEM characterization studies were carried out by applying an accelerating voltage of 5 kV, a beam current of 20 mA and a probe current of 30 pA. r-Filter was applied to combine signals (1[thin space (1/6-em)] : [thin space (1/6-em)]1) from secondary and backscattered electrons. The thicknesses of TiN thin films were measured and statistically evaluated using proprietary Nanomeasure software.

The roughness of all substrates coated with TiN using 100c, 200c, 300c and 400c was determined by Atomic Force Microscopy (AFM, Bruker Dimension FastScan) on an area of 1 × 1 sq. μm. Scanasyst-Air tips (f_0 = 70 kHz) were used. The average roughness values are calculated from 5 different scans on each sample.

X-Ray photoelectron spectroscopy (XPS, Kratos Axis Supra) was used to evaluate the surface chemical composition of all TiN films. A monochromatic Al Kα (1486.7 eV) X-ray source operated at 250 W was employed. Depth profiling on Si wafer coated with 400c ALD TiN was performed using Ar^+ ion flux sputtering (5 keV) with 3 × 3 mm sq. cluster size for a total of 42 min with each sputtering duration of 3 min. Additionally, the rate of surface oxidation was studied by XPS on 100c, 200c, 300c and 400c ALD TiN exposed for 0 h, 48 h, 1 week, 3 weeks, 11 weeks and 16 weeks. The binding energy scale was not referenced to adventitious carbon (284.8 eV); instead the signal of Ti–N at 454.9 eV was used, due to the sputtering experiments, where the carbon signal disappeared. Analysis of data was done using CasaXPS software, and the elemental sensitivity factors provided by the manufacturer were used for the quantitative analysis. Ti 2p spectra were fitted using the Shirley-type background, asymmetric Lorentzian functions LA (0.98, 2, 150) for the Ti–N components and mixed Gaussian–Lorentzian functions GL (30) for oxynitride, oxide and satellite peaks. The area ratio 2 : 1 and the binding energy distance constraints between the spin–orbit splitting (Ti $2p_{3/2}$ and Ti $2p_{1/2}$) 6.0 eV for Ti–N

Table 1 Parameters for scratch measurements on Si wafer coated with 100c, 200c, 300c and 400c ALD TiN

	Parameter	Value	Unit
Type	Progressive	—	—
Loading	Scanning load	0.03	mN
	Begin load	0.03	mN
	End load	10	mN
	Loading rate	19.94	mN min^{-1}
Displacement	Speed	400	μm min^{-1}
	Length	200	μm min^{-1}

species, 5.7 eV for oxides and 5.0 eV for shake-up satellites, were considered.

X-ray diffractometry (XRD) was performed using a Pan-alytical Empyrean with a Cu tube and a Pixcel3D detector. Grazing incidence X-ray diffraction was performed to obtain the diffraction patterns of the as-deposited 100c, 200c, 300c and 400c ALD TiN thin films on all substrates. The incident angle was 1°. The patterns were recorded in the 2θ range of 5–65°, the step size was 0.026°, and the time per step was 11 s.

The four-probe electrical characterization was performed on glass samples (unexposed) and coated with TiN using 100c, 200c, 300c and 400c with a custom-made box equipped with a head containing 4 probes arranged in line with 1 mm spacing in combination with a Keithley 2401 Source Meter. A standard method was employed, where outer probes were supplying the current, while the inner probes measured the voltage difference. The optimal measuring current of 30 mA was experimentally determined for all samples according to current sweeping in the range from 0 to 100 mA with a step of 5 mA. Additionally, the same set of samples were exposed to the atmosphere for 48 h, 1 week, 3 weeks, 11 weeks, and 16 weeks to study the influence of the potential surface oxidation on the sheet resistance. Three measurements were performed on each sample at different places to obtain data for the calculation of the mean value and standard deviation.

The scratch measurements on Si wafers coated with TiN using 100c, 200c, 300c and 400c were carried out using a high-resolution cantilever on an NST3 tester (Nanoscratch Tester) by Anton Paar. A 2 μm radius indenter was used for the same with the test parameters mentioned in Table 1.

3. Results and discussion

Fig. 1 shows top-view SEM images of ultrathin TiN ALD films, prepared using 100c, 200c, 300c and 400c on Si wafers, soda lime glasses and Ti foil. Additional SEM images for all uncoated and ALD TiN coated substrates at lower magnification are shown in Fig. S2. No significant differences between samples prepared by different numbers of ALD cycles can be observed in the case of Si wafers. There is an island growth of ALD TiN deposited on Si wafers, beyond the nucleation stage (typically around 1–3 nm). Furthermore, with higher thickness, the morphology evolves into polycrystalline films with distinct islands observable.[41] In contrast, particle-like structures are visible on the soda lime glasses coated with ALD TiN. Although the reason behind these structures is unknown, a trend in the size and density of the particles can be observed at lower magnification, as shown in Fig. S2. While the size of the particles decreases, the density increases with the higher number of ALD TiN cycles. Last but not least, in the case of Ti foil, which is by far not as planar, there are numerous small metallic islands/bumps that become overcoated and increase their overall size with a higher number of ALD TiN cycles. These islands/bumps on Ti foil have already been there before any ALD process, as shown in Fig. S2.
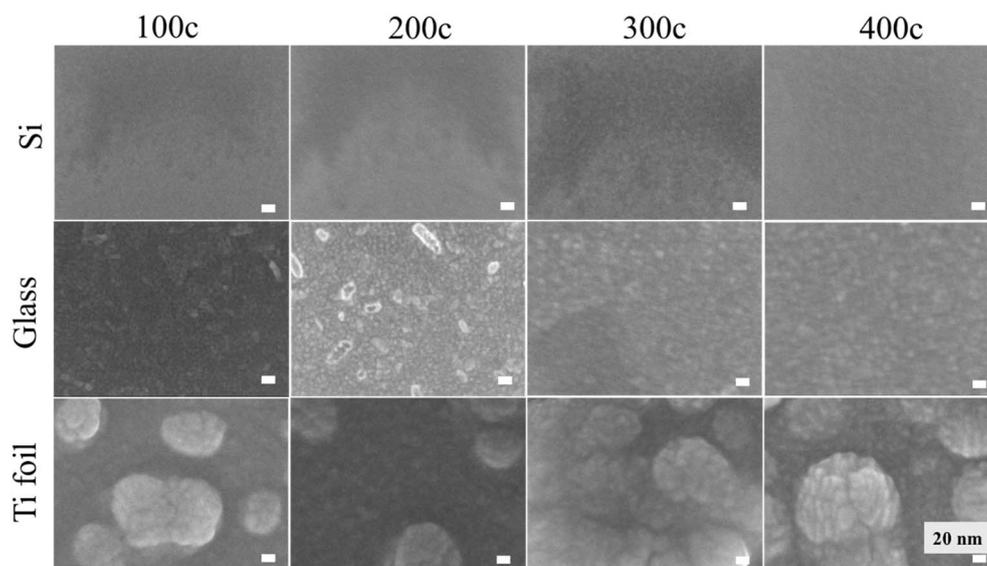

Fig. 1 SEM top-view images of a Si wafer, soda lime glasses and Ti foil coated with 100c, 200c, 300c and 400c ALD TiN, respectively. Scale bars represent 20 nm.

From the AFM images shown in Fig. 2 in the same layout as used for the SEM images in Fig. 1, the island/grain structures are visible in all substrates, coated with ALD TiN. The images reveal a transition from a lower to a higher number of distinct grains with increasing number of ALD cycles.

To gain additional evidence on roughness, Root-Mean-Square (RMS) values were calculated from 5 scans at different areas. The results are shown in Fig. 3 in the form of box plots.

These plots show significantly lower RMS values of control/ uncoated samples of each type, which is expected. The trend of increasing roughness indicates the grain growth and surface reconstruction, with roughness reflecting the surface morphology changes seen in SEM and AFM images in Fig. 1 and 2, respectively. The average roughness increased from 2.8 nm to ~6.1 nm in the case of Si wafers. This implies that the very flat surface of a Si wafer promotes the growth of relatively smooth TiN ultrathin films with gradual roughening, as the number of ALD cycles increased. The roughness increased progressively and steadily from control to 400c ALD TiN. Similarly, the trend of increase in roughness of soda lime glasses fits well with the SEM results. With the increasing density of particles with more ALD cycles, the roughness increases on soda lime glasses from 1.2 nm for control samples to 8.6 nm for ALD of TiN using 400c. The formation of particles/grain like structures on a Si wafer and soda lime glass can be due to the mismatch in crystal structure of these substrates and ALD TiN films.[42] The Ti foil surface with 400c ALD TiN showed the highest average RMS value (~80 nm) among all substrates and cycle numbers, indicating large grain formations and more significant surface texture changes. These RMS roughness trends confirmed the influence of both the substrate type and the number of ALD cycles on surface morphology and roughness of TiN ultrathin

films. This has practical implications in tailoring the surface properties like adhesion, wear resistance and others.

The crystallinity and preferred orientations of ALD TiN films on all substrates were characterized by X-ray diffractometry. The intensity and sharpness of the peaks turned out to be influenced by different substrates. On Si wafers, as shown in Fig. 4a, the presence of rather broad (111), (020) and (022) diffraction peak reflections was revealed, corresponding to the $Fm\bar{3}m$ (cubic) group of TiN with a lattice parameter of 4.2213 Å, with moderate broadening signal formation of polycrystalline films. On soda lime glasses, as shown in Fig. 4b, TiN peaks were also rather broader, suggesting a nanocrystalline character of TiN. The presence of characteristic diffraction peaks of TiN, (111) at $\approx 36.85°$, (200) at $\approx 42.81°$, and (220) at $\approx 62.15°$ confirmed the crystallinity of the as-deposited ultrathin films.[23,41] Finally, on Ti foil, as shown in Fig. 4c, these diffraction peaks were also revealed, but sharper and more intense.

Only in the case of Si wafers and soda lime glasses with 100c ALD TiN, the XRD patterns show rather weak, broad, or even absent TiN reflections. This indicates less pronounced crystallinity, smaller grain size, or a partially amorphous structure. In contrast, for 200c, 300c, and 400c ALD TiN, the peaks are sharper and more intense, which directly reflects improved crystallinity, preferred orientation, and an increase in average grain size. This corresponds to a general trend that increased film thickness provides a better environment for crystal growth and strain relaxation.

XPS depth profiling on Si wafers with 400c ALD TiN was used to study the variation of elemental composition, chemical states, and thickness-dependent properties across the thickness of the TiN film. Fig. 5a shows the atomic concentration (%) for C, N, O, Ti and Si as a function of the sputtering time. At the very
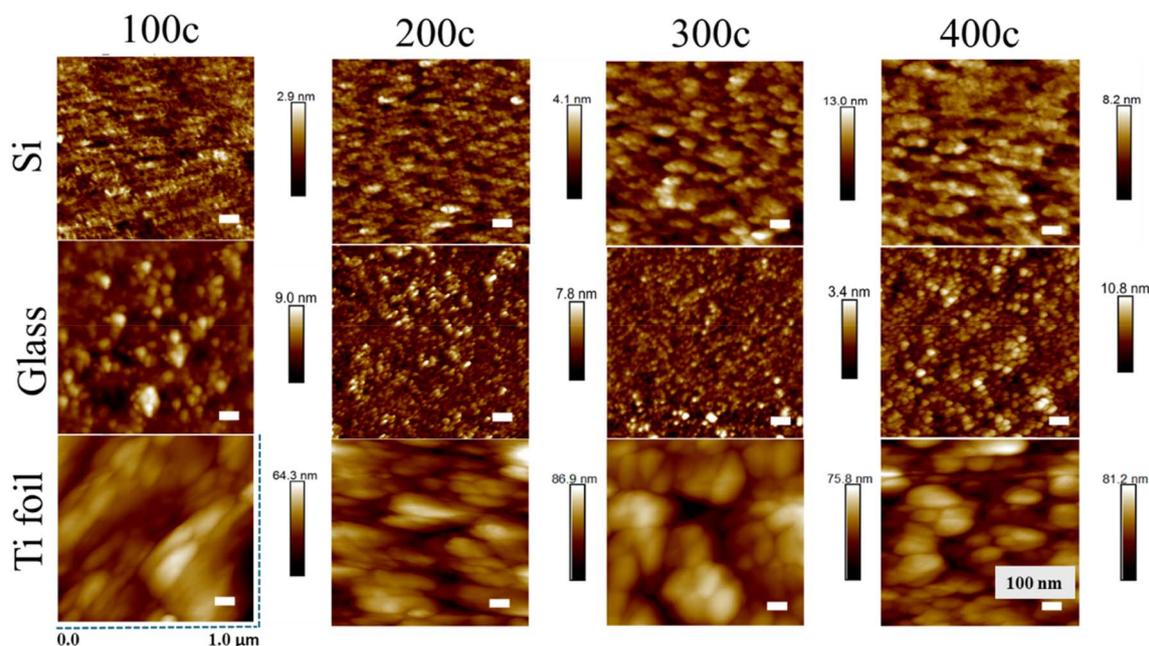

Fig. 2 AFM scans (across 1 × 1 sq. μm) for Si wafers, soda lime glasses and Ti foil coated with ALD TiN using 100c, 200c, 300c and 400c, respectively. Scale bars represent 100 nm.
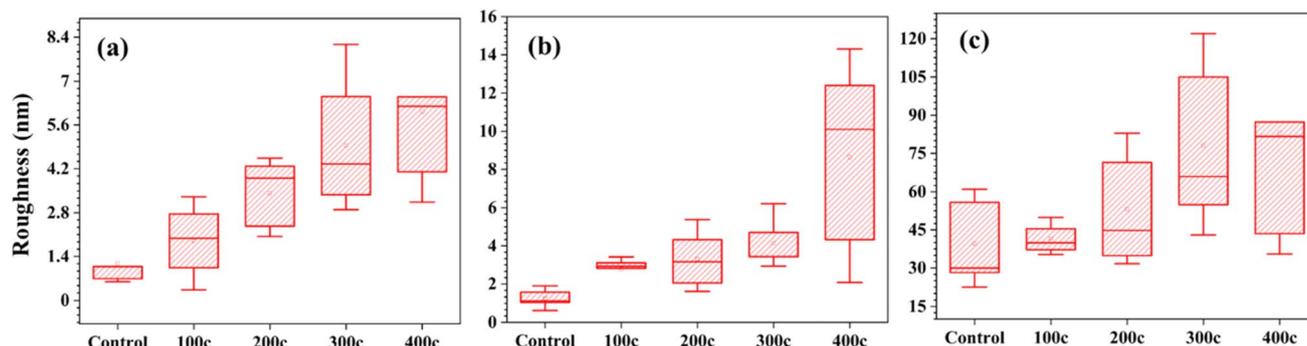
Fig. 3 Roughness values (root mean square, RMS), obtained by AFM in the form of the box-plot for (a) Si wafers, (b) soda lime glasses and (c) Ti foil coated with TiN ALD films using 100c, 200c, 300c and 400c.
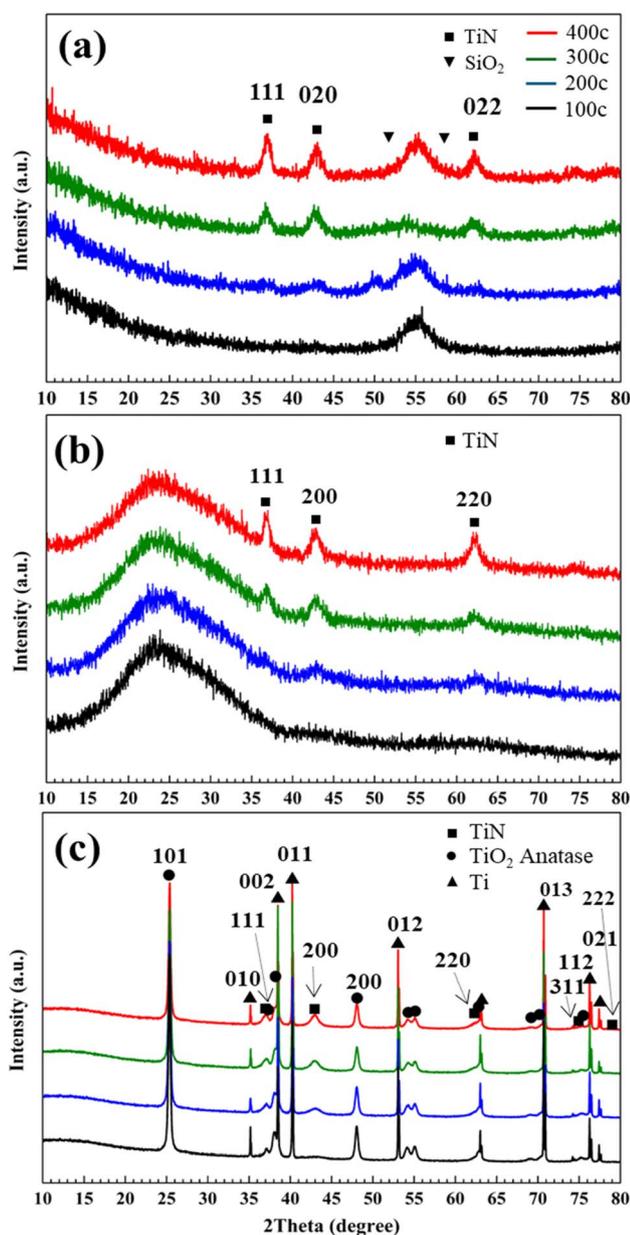

Fig. 4 XRD patterns of ALD TiN films deposited on (a) Si wafers, (b) soda lime glasses and (c) Ti foil. Peaks for individual planes of TiN peaks are assigned in (c).

onset, an O concentration of ~18% was recorded, which had a decreasing trend during the sputtering period. During the initial sputtering duration of 0–6 min, Ti and N concentrations were approx. 40% and followed the same trend. This equal percentage confirms rather stoichiometric TiN near the surface, as expected for ALD TiN films. Simultaneously, O is also present at the surface (~18–20%) of the unexposed (0 h) sample. However, the C signal disappears during the initial minutes of sputtering. The Si concentration from the substrate was 0% until 6 min of sputtering, indicating effective coverage by TiN with little breakthrough from the substrate. A sharp increase in the Si concentration begins at 9 min and at around 24 min rapidly climbs to ~90% indicating the approach to the Si wafer surface, as the TiN film was sputtered through. The Ti and N also fall off gradually from ~32% after 9 min to ~4% after 27 min of sputtering. O also decreases gradually after 9 min of sputtering, consistent with the removal of the oxide-rich surface and transition into the substrate. This profile confirms a uniform and well-controlled ALD TiN deposition on Si wafer surfaces. The surface O (and minor C) content indicates typical air-exposure and adventitious contamination occurring before the measurement (sputtering), not intrinsic to TiN. The depth-profile in Fig. 5a strongly supports that effective ALD TiN deposition was achieved on the Si wafer surface, with a sharp interface and stoichiometric surface coverage, verified by elemental XPS signals as a function of the sputtering time.

To gain better insights into the surface chemical state evolution of the ALD TiN 400c film, the high-resolution Ti 2p XPS spectra with their characteristic spin–orbit splitting of Ti $2p_{3/2}$ and Ti $2p_{1/2}$ were peak fitted on three different sputtering stages (0, 12 and 36 min). The results are shown in Fig. 5b–d. At 0 min of sputtering the Ti 2p spectrum was curve fitted using 8 components, which correspond to three different chemical environments and one pair of characteristic TiN satellites (Fig. 5b). The first doublet (red peaks) centered at ~454.9 and 460.9 eV was related to Ti–N bonds. The second pair of components (blue peaks) located at ~456.1 and 461.8 eV was attributed to Ti–O–N species (TiO_xN_y). The broader olive peaks were associated with the TiN shake-up satellites at ~456.9 and 461.9 eV. Finally, the contribution of the orange doublet, assigned to Ti–O bonds (TiO_2) was found at ~458.1 and
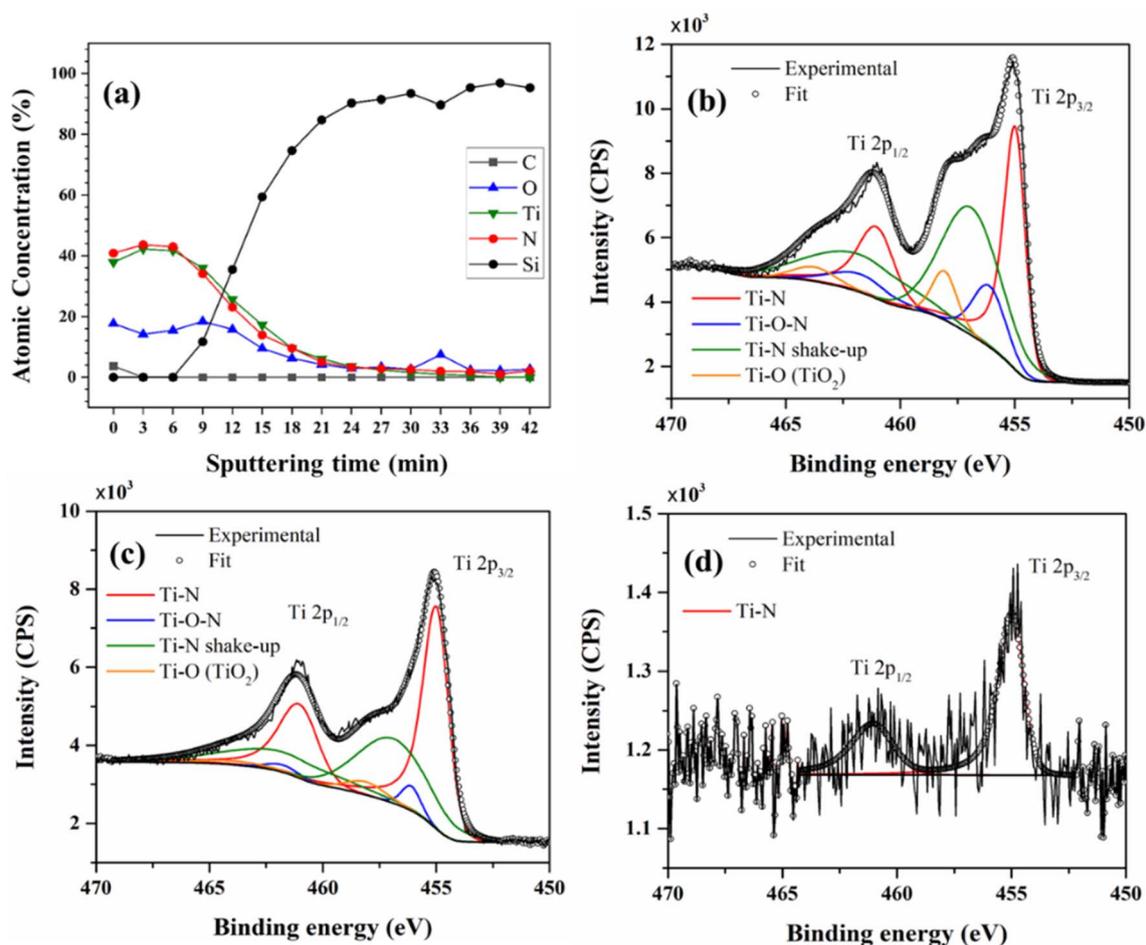
Fig. 5 (a) XPS depth profile of 400c ALD TiN on Si wafers; a change in atomic concentration (%) *vs.* sputtering time and evolution of the Ti 2p peak after (b) 0 min, (c) 12 min and (d) 36 min of sputtering.

463.8 eV. After 12 min of sputtering as shown in Fig. 5c, the peak fitted Ti 2p spectra exhibited the same chemical species as the as-deposited. However, the intensity of the components related to oxides species, namely TiO_xN_y and TiO_2 notably decreased. Upon further sputtering (36 min), as shown in Fig. 5d TiN is nearly fully removed, and hence, the signal weakens due to thinning and an increasing substrate influence. At 24 min (data not shown) no new distinct species compared to 36 min of sputtering (Fig. 5d) appeared.

The influence of the surface oxidation upon extensive exposure time under ambient conditions (*i.e.* laboratory air) on 100c, 200c, 300c and 400c ALD TiN films, coated on soda lime glasses, is shown in Fig. 6. The recorded initial O concentrations, obtained for 100c, 200c, 300c and 400c, are approx. 30%, 20%, 21% and 18%, respectively. Additionally the respective thicknesses for 100c, 200c, 300c and 400c ALD TiN are 4.7, 9.4, 14.1 and 18.8 nm (as calculated from the measured growth rate from Fig. S1). The reason for the lowering of O content with increased ALD cycles is that XPS measures the top ~5–10 nm; hence the Ti-oxide signal dominates the thinner films, but the Ti-oxide signal gets averaged with a much larger low-oxygen TiN signal as films thicken, lowering the overall oxygen percentage seen by

XPS. Moreover, the change in atomic concentration of C, N, O, and Ti can be clearly observed between different exposure times in air: time 0 (unexposed), 48 h, 1 week, 3 weeks, 11 weeks and 13 weeks. The "others" represent the combined concentration of elements related to the substrate. This might be due to an oxide layer, formed upon exposure to ambient conditions, that constitutes a larger fraction of the total film thickness in thinner ALD TiN films, resulting in a higher overall O 1s signal.[5] It is clear from these results that all ALD TiN films accumulate oxygen and moisture after exposure, allowing oxygen atoms to react with the TiN surface, forming TiO_2 and oxynitride species.

The O concentration increases slightly during the ambient-air exposure from 0 h to 16 weeks, due to the low rate of surface oxidation. However, the rate of oxidation seems to stabilize over the course of time, possibly due to the passivation effect of the oxide layer on the TiN surface, which is common with transition metal nitrides and oxides.[43] Overall, the surface oxidation occurs at a steady rate, over different exposure periods, but an increasing C contamination was also observed. The initial N concentrations recorded at 0 h for 100c, 200c, 300c and 400c ALD TiN were ~19%, ~27, ~29% and 30% respectively. The N concentrations gradually decreased in the case of
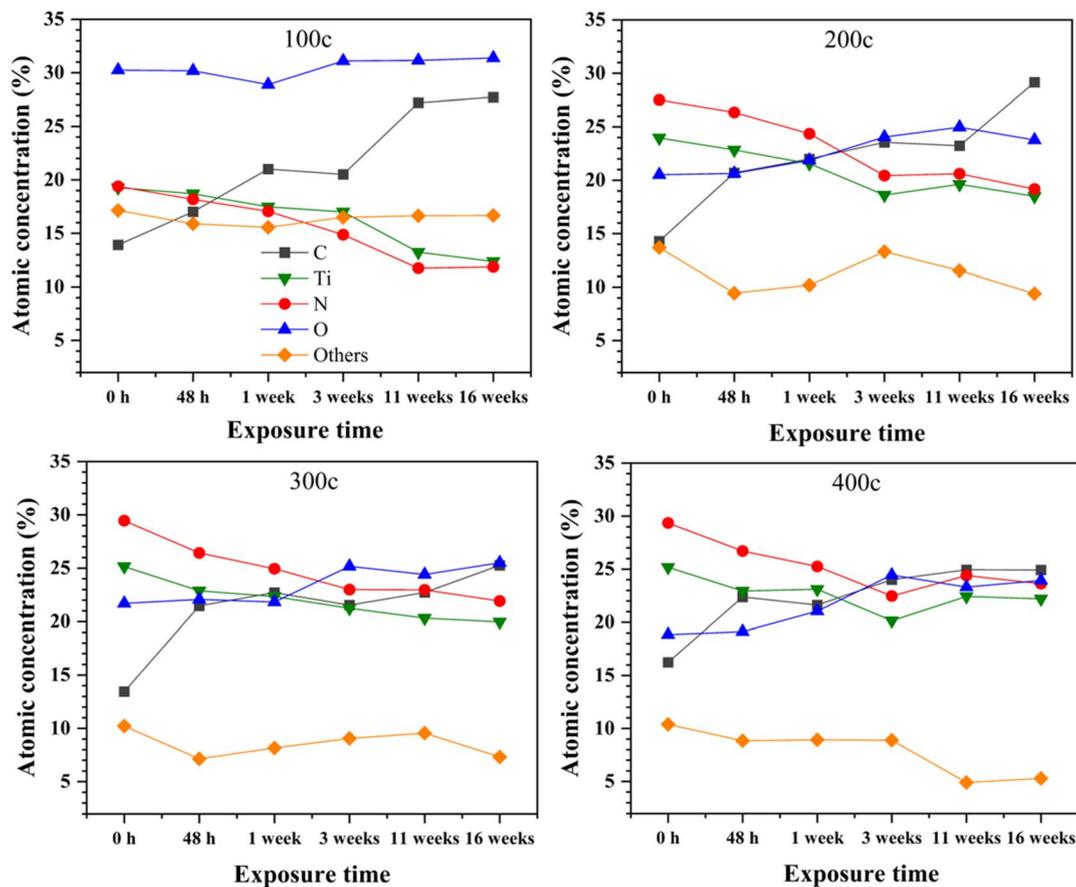
Fig. 6 Variation of atomic concentrations of C, O, Ti, and N species as a function of exposure times, determined by XPS for 100c, 200c, 300c, and 400c of ALD TiN on soda lime glasses.

100c and 200c ALD TiN with the exposure time, implying that TiN is partially converted to TiO_2 by replacement or coverage of nitrogen. The thicker ALD TiN films (300c and 400c) retained high N concentration and stabilize around 23% at longer exposures, probably due to improved coverage and resistance to ambient conditions. Similar to N, Ti concentrations recorded at 0 h range from ~19 to ~25% at 16 weeks, indicating a dense TiN film structure. Although a gradual decrease in Ti concentrations is observed in all cases, the decrease is more evident for 100c and 200c ALD TiN. This is possibly due to easier penetration of ambient oxygen and moisture into these thinner films, as also indicated by relatively high elemental concentrations (predominantly Si from the substrate) of ~18% and 13%, respectively. Overall, the Ti and N concentrations are more stable (Ti: ~25–19%; N: ~29–21%) during the entire exposure period, indicating that increased ALD cycles preserve the TiN stoichiometry better during the ambient exposure.

In addition to long-term observation of the composition by XPS, the sheet resistance of 100c, 200c, 300c, and 400c of ALD TiN on soda lime glasses was also investigated as a function of different exposure times. The results are shown in Fig. 7. Unexposed (marked as 0 h) 400c ALD TiN exhibited the best sheet resistance (287 Ω/□) across all samples and times. At 0 h of exposure, 100c ALD TiN showed the highest sheet resistance

at ~222.3 kΩ/□ compared to 200c (2.5 kΩ/□), 300c (519 Ω/□) and 400c (287 Ω/□) at the same exposure time. This trend of decreasing sheet resistance with higher ALD TiN cycles was retained throughout the entire data set. The lowest resistivity achieved in this work – 540 μΩ.cm – for 400c (as a result of multiplying 287 Ω/□ with 18.8 nm of thickness) is very comparable to that in other publications. A comparative table (Table S1) for different ALD processes used for preparing TiN thin films, in terms of precursors, growth rate and resistivity is provided in the SI.

As shown in Fig. 6, gradual oxidation was observed (1 week to 3 weeks) in the case of 200c, 300c and 400c samples, and a similar trend was also evidenced in the increase in sheet resistance. During that transition period, sheet resistance increases from 2.6 kΩ/□ to 2.9 kΩ/□ for 200c, 518 Ω/□ to 550 Ω/□ for 300c and 295.10 Ω/□ to 299.1 Ω/□ for 400c ALD TiN. However, the sudden change in the sheet resistance for 100c ALD TiN coated soda lime glass after 11 weeks is somewhat unexpected and can be assigned to potential crack/damage due to repeated probing during the measurements. In the remaining time period (11 or 16 weeks), the sheet resistance further increased or leveled-off, depending on the particular film.

Additionally, the mechanical properties of the TiN ultrathin films were investigated. Scratch test results on uncoated and Si
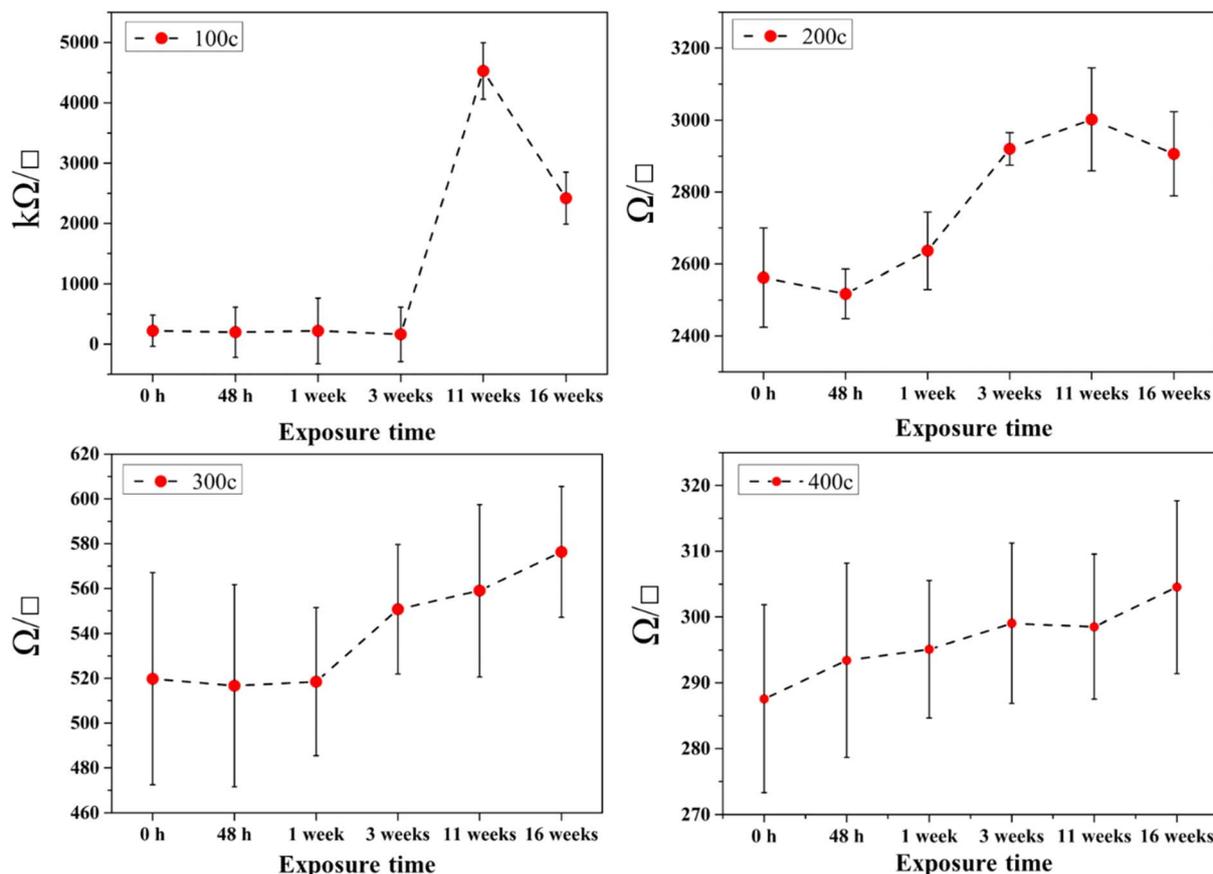
Fig. 7 The sheet resistance of 100c, 200c, 300c and 400c of ALD TiN films on soda lime glasses, evaluated by 4-probe measurements.

wafers coated with TiN ALD films using 100c, 200c, 300c and 400c are shown in Fig. 8. The scratches visible as straight lines were made as the stylus on the indenter moved at a constant velocity, while linearly increasing the applied force. Hence, the longer the scratch, the higher the stability of the TiN ultrathin film with increasing mechanical force before failure. According to the data obtained, 100c ALD TiN was scratched with Lc = 7.9

mN, very similar to 7.6 mN and 7 mN for 300c and 400c ALD TiN coated Si wafers, respectively. However, for 200c ALD TiN the recorded Lc is 5.8 mN which shows that from Fig. 8 no specific trend of Lc *vs.* ALD TiN cycles can be concluded. Due to the thinness of the ALD TiN films on all the samples, no visible delamination occurred and was visible. However, there is a difference in the point at which scratching becomes evident
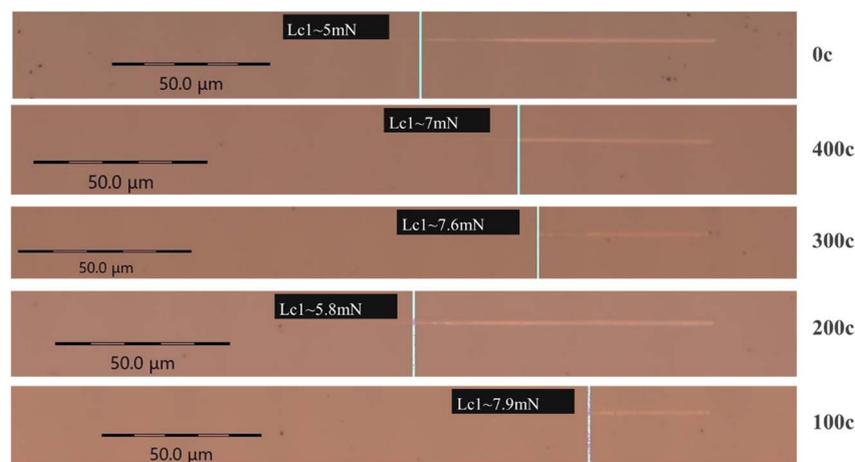

Fig. 8 Panoramic picture of the scratches during the scratch measurements on uncoated Si wafers and wafers coated with 100c, 200c, 300c and 400c ALD TiN. Lc1 = critical load.

between the samples. It appears that this threshold is lower for the sample without the TiN film, suggesting that the presence of the ALD TiN film influences the scratch resistance of the samples. It is important to note that the values across the different samples are very close, and there is no clear relationship between the film thicknesses and the critical load (Lc) values.

4. Conclusions

TiN ultrathin films of different thicknesses were deposited on Si wafers, soda lime glasses and Ti foils using ALD and varying numbers of ALD cycles (100, 200, 300 to 400 ALD cycles). For that, $TiCl_4$ and NH_3 were used as Ti and N precursors, respectively. The deposition rate of ALD TiN at 400 °C was $\approx$ 0.047 nm per cycle. This nominally yielded TiN film thickness of 4.7, 9.4, 14.1 and 18.8 nm, respectively. XRD patterns confirmed the formation of cubic TiN, with increasing crystallinity and preferred orientation as the cycles increased, notably enhanced on Ti foil and Si wafers, compared to glass. The lattice parameter remained close to the standard value of 4.221 Å, indicating high-quality crystalline TiN phase formation. The XPS depth profiling, performed on Si wafers coated with 400c ALD TiN films showed the quality, chemical environment and evolution of the TiN film with the sputtering time. The TiN films coated with different numbers of ALD cycles were exposed to ambient air for different times. The XPS depth profiles revealed that the thicker films (200c, 300c and 400c) exhibited lower overall O content, due to the reduced relative influence of this surface oxide and improved film density. In terms of mechanical behaviour of the TiN films, scratch tests showed that the critical load for film failure increased from approximately 5 mN for the uncoated Si wafers to around 7–8 mN for the ALD TiN coated ones, reflecting an enhanced adhesion and a scratch resistance. In terms of the sheet resistance, the 400c ALD TiN film with a thickness of $\sim$18.8 nm showed the lowest sheet resistance of 287 $\Omega/\square$. This comprehensive dataset highlights that increasing ALD cycles enhances TiN film crystallinity, reduces surface oxidation effects, and improves mechanical robustness, underscoring the importance of optimizing TiN film thickness and substrate choice for targeted applications.

Author contributions

Kaushik Baishya: ALD film characterization (including AFM, XPS, and sheet resistance measurements), data analysis and drafted the manuscript. Luděk Hromádko: SEM and XRD characterization, assisted in data interpretation, and revised the manuscript. Jan Brodský: contributed to electrical characterization experiments, interpretation of sheet resistance data, and critical revision of the manuscript. Jhonatan Rodriguez-Pereira: ALD processes, contributed to the optimization of ALD processing parameters, assisted in XPS data analysis, and manuscript editing. Raul Zazpe: ALD processes, contributed to the optimization of ALD processing parameters, conceived and supervised the ALD experiments, contributed to data interpretation, and critically revised the manuscript. Jan M. Macak:

coordinated the overall project, contributed to the experimental design, and interpretation of the mechanical performance and durability results, and provided critical revisions to the manuscript. All authors discussed the results and approved the final version of the manuscript.

Conflicts of interest

There are no conflicts to declare.

Data availability

All data supporting this article are available in the supplementary information (SI). Supplementary information: SEM images of TiN layers, comparative table of ALD processes in terms of precursors, growth rate and resistivity. See DOI: https://doi.org/10.1039/d5na01134e.

Acknowledgements

References

1 L. Toth, *Transition Metal Carbides and Nitrides*, Elsevier Science, 2014.

2 M. Hua, H. Y. Tam, H. Y. Ma and C. K. Mok, *Wear*, 2006, **260**, 1153–1165.

3 R. Fix, R. G. Gordon and D. M. Hoffman, *Chem. Mater.*, 1991, **3**, 1138–1148.

4 J. Uhm and H. Jeon, *Jpn. J. Appl. Phys.*, 2001, **40**, 4657–4660.

5 S. Kaskel, K. Schlichte and T. Kratzke, *J. Mol. Catal. A Chem.*, 2004, **208**, 291–298.

6 B. M. Biwer and S. L. Bernasek, *Appl. Surf. Sci.*, 1986, **25**, 41–52.

7 M. Al-Dhaifallah, M. A. Abdelkareem, H. Rezk, H. Alhumade, A. M. Nassef and A. G. Olabi, *Int. J. Energy Res.*, 2021, **45**, 1587–1598.

8 J. A. DeWitt, E. V. Phillips, K. L. Hebisch, A. W. Tricker and C. Sievers, *Faraday Discuss.*, 2022, **243**, 65–76.

9 G. V. Naik, J. L. Schroeder, X. Ni, A. V. Kildishev, T. D. Sands and A. Boltasseva, *Opt. Mater. Express*, 2012, **2**, 478.

10 T. S. Kim, S. S. Park and B. T. Lee, *Mater. Lett.*, 2005, **59**, 3929–3932.

11 A. Jafari, Z. Ghoranneviss, A. S. Elahi, M. Ghoranneviss, N. Fasihi Yazdi and A. Rezaei, *Adv. Mech. Eng.*, 2014, **6**, 373847.

12 G. V. Naik, B. Saha, J. Liu, S. M. Saber, E. A. Stach, J. M. K. Irudayaraj, T. D. Sands, V. M. Shalaev and A. Boltasseva, *Proc. Natl. Acad. Sci. U. S. A.*, 2014, **111**, 7546–7551.

13 S. Prayakarao, S. Robbins, N. Kinsey, A. Boltasseva, V. M. Shalaev, U. B. Wiesner, C. E. Bonner, R. Hussain, N. Noginova and M. A. Noginov, *Opt. Mater. Express*, 2015, **5**, 1316.

14 Y. Krockenberger, S. I. Karimoto, H. Yamamoto and K. Semba, *J. Appl. Phys.*, 2012, **112**(8), DOI: 10.1063/1.4759019.

15 W. P. Guo, R. Mishra, C. W. Cheng, B. H. Wu, L. J. Chen, M. T. Lin and S. Gwo, *ACS Photonics*, 2019, **6**, 1848–1854.

16 H. E. Rebenne and D. G. Bhat, *Surf. Coat. Technol.*, 1994, **63**, 1–13.

17 R. Fix, R. G. Gordon, D. M. Hoffman and E. O. Sherman, Transition Metal Carbides and Nitrides, *J. Vac. Sci. Technol., B:Microelectron. Nanometer Struct.-Process., Meas., Phenom.*, 1991, **3**, 1138–1148.

18 J. Su, R. Boichot, E. Blanquet, F. Mercier and M. Pons, *CrystEngComm*, 2019, **21**, 3974–3981.

19 J. Zhao, E. G. Garza, K. Lam and C. M. Jones, *Appl. Surf. Sci.*, 2000, **158**, 246–251.

20 C. Faltermeier, C. Goldberg, M. Jones, A. Tlpham, D. Manger, G. Peterson, J. Lau, A. E. Kaloyeros, B. Arkles and A. Paranjpea, *Barrier Properties of Titanium Nitride Films Grown by Low Temperature Chemical Vapor Deposition from Titanium Tetra Iodide*, The Electrochemical Society, Inc, 1997, vol. 144, pp. 1002–1008.

21 A. Valour, M. A. U. Higuita, G. Guillonneau, N. Crespo-Monteiro, D. Jamon, M. Hochedel, J. Y. Michalon, S. Reynaud, F. Vocanson, C. Jiménez, M. Langlet, C. Donnet and Y. Jourlin, *Surf. Coat. Technol.*, 2021, **413**, 127089.

22 B. Lee Sang, M.-J. Gour, M. Darnon, S. Ecoffey, A. Jaouad, B. Sadani, D. Drouin and A. Souifi, *J. Vac. Sci. Technol., B:Nanotechnol. Microelectron.:Mater., Process., Meas., Phenom.*, 2016, **34**(2), DOI: 10.1116/1.4936885.

23 C. H. Ahn, S. G. Cho, H. J. Lee, K. H. Park and S. H. Jeong, *Characteristics of TiN Thin Films Grown by ALD Using TiCl 4 and NH 3*, 2001, vol. 7.

24 K. Kawata, H. Sugimura and O. Takai, *Thin Solid Films*, 2002, **407**, 38–44.

25 U. Mahajan, M. Dhonde, K. Sahu, P. Ghosh and P. M. Shirage, *Mater. Adv.*, 2024, **5**, 846–895.

26 A. Matthews and A. R. Lefkow, *Thin Solid Films*, 1985, **126**, 283–291.

27 D.-J. Kim, Y.-B. Jung, M.-B. Lee, Y.-H. Lee, J.-H. Lee and J.-H. Lee, *Applicability of ALE TiN Films as CurSi Diffusion Barriers*, 2000, vol. 372.

28 M. Ritala, M. Leskelä, E. Rauhala and P. Haussalo, *J. Electrochem. Soc.*, 1995, **142**, 2731–2737.

29 J. Musschoot, Q. Xie, D. Deduytsche, S. Van den Berghe, R. L. Van Meirhaeghe and C. Detavernier, *Microelectron. Eng.*, 2009, **86**, 72–77.

30 J. Kim, H. Hong, S. Ghosh, K. Y. Oh and C. Lee, *Jpn. J. Appl. Phys.*, 2003, **42**, 1375–1379.

31 C. H. Kuo, A. J. Mcleod, P. C. Lee, J. Huang, H. Kashyap, V. Wang, S. U. Yun, Z. Zhang, J. Spiegelman, R. Kanjolia, M. Moinpour and A. C. Kummel, *ACS Appl. Electron. Mater.*, 2023, **5**, 4094–4102, DOI: 10.1021/acsaelm.3c00245.

32 H. Cho, B. Nie, A. Dhamdhere, Y. Meng, M. Neuburger, J. H. Ahn, S. H. Jung and H. Y. Kim, *Mater. Lett.*, 2021, **291**, 129554.

33 M. Sepúlveda, J. Capek, K. Baishya, J. Rodriguez-Pereira, J. Bacova, S. Jelinkova, R. Zazpe, H. Sopha, T. Rousar and J. M. Macak, *Front. Bioeng. Biotechnol.*, 2024, **12**, 1515810.

34 R. Zazpe, J. Charvot, J. Rodriguez-Pereira, L. Hromádko, M. Kurka, K. Baishya, H. Sopha, F. Bureš and J. M. Macak, *Nanoscale*, 2025, **17**, 12406–12415.

35 R. Zazpe, M. Knaut, H. Sopha, L. Hromadko, M. Albert, J. Prikryl, V. Gärtnerová, J. W. Bartha and J. M. Macak, *Langmuir*, 2016, **32**, 10551–10558.

36 K. Baishya, J. Bacova, B. Al Chimali, J. Capek, J. Michalicka, G. Gautier, B. Le Borgne, T. Rousar and J. M. Macak, *ACS Appl. Mater. Interfaces*, 2025, **17**, 739–749.

37 J. Kim, H. Hong, K. Oh and C. Lee, *Appl. Surf. Sci.*, 2003, **210**, 231–239.

38 S. Wolf, M. Breeden, I. Kwak, J. H. Park, M. Kavrik, M. Naik, D. Alvarez, J. Spiegelman and A. C. Kummel, *Appl. Surf. Sci.*, 2018, **462**, 1029–1035.

39 J. Fammels, P. C. Lee, D. Pal, J. Pilz, D. Solonenko, J. Spiegelman and A. C. Kummel, in *2024 IEEE International Interconnect Technology Conference, IITC 2024*, Institute of Electrical and Electronics Engineers Inc., 2024.

40 J. Femi-Oyetoro, S. Sypkens, H. LeDuc, M. Dickie, A. Beyer, P. Day and F. Greer, *Appl. Phys. Lett.*, 2024, **125**(6), 62601.

41 H. Van Bui, *Atomic layer deposition of TiN films: growth and electrical behavior down to sub-nanometer scale*, University of Twente, 2013.

42 K. B. Klepper, O. Nilsen and H. Fjellvåg, *Thin Solid Films*, 2007, **515**, 7772–7781.

43 H. Van Bui, A. W. Groenland, A. A. I. Aarnink, R. A. M. Wolters, J. Schmitz and A. Y. Kovalgin, *J. Electrochem. Soc.*, 2011, **158**, H214.